

Network localization strength regulates innovation diffusion with macro-level social influence

Leyang Xue¹, Kai-Cheng Yang², Peng-Bi Cui^{*1}, and Zengru Di¹

¹International Academic Center of Complex Systems, Beijing Normal University, Zhuhai, 519087, China

²Luddy School of Informatics, Computing, and Engineering, Indiana University, Bloomington, Indiana 47408, USA

Abstract

Innovation diffusion in the networked population is an essential process that drives the progress of human society. Despite the recent advances in network science, a fundamental understanding of network properties that regulate such processes is still lacking. Focusing on an innovation diffusion model with pairwise transmission and macro-level social influence, i.e., more adopters in the networked population lead to a higher adoption tendency among the remaining individuals, we observe discontinuous phase transitions when the influence is sufficiently strong. Through extensive analyses of a large corpus of empirical networks, we show that the tricritical point depends on the network localization strength, which our newly proposed metric can effectively quantify. The metric reveals the deep connection between the critical and tricritical points and further indicates a trade-off: networks that allow less attractive products to prevail tend to yield slower diffusion and lower market penetration and vice versa. Guided by this trade-off, we demonstrate how marketers can rewire the networks to modulate product diffusion according to their needs.

The dissemination of new ideas, technology, and products, or innovation diffusion, is a fundamental process that drives the socioeconomic development of our society. Identifying the factors that affect such processes and analyzing their unique mechanism can yield invaluable insights and guide marketing strategies and policy-making [1]. Since it encompasses complex social processes such as interpersonal communication, social learning, decision-making, and social contagion, innovation diffusion has drawn strong research interest from various fields including management, economics, sociology, psychology, and physics [2, 3, 4]. Due to the difficulty of excluding the effects of confounding factors in empirical studies, many researchers resort to the modeling approach [5, 6].

Naturally, the inherent characteristics of the technology or products and the psychology of the consumers can exert a strong impact on the diffusion process [7]. But many recent empirical and simulation studies highlight the critical role played by the connectivity pattern of the target population [8, 9, 10]. For instance, some structural features of networked population, such as heterogeneity and clustering, can largely shape the product dissemination process [11, 12]. The hubs in the networks are of particular interest since they play

*cuisir610@gmail.com

a key role in promoting the product [13, 14]. Such findings are not surprising since it is well-known in network science that underlying topological structures can strongly affect all dynamical processes [15, 16]. However, a fundamental understanding of network properties that regulate the innovation diffusion process is still lacking and we aim to close this gap in this paper.

Following the recent trend in innovation diffusion modeling studies [12], we consider the dissemination process of a new product in a networked population with social influence at different levels. The micro-level influence is conveyed through pairwise interaction between neighbors in the network [17] and represents mechanisms such as the well-documented word-of-mouth effect [18]. The macro-level influence increases the tendency of individuals to adopt the new product as market penetration increases. Such influence is essentially a positive feedback mechanism between the macro system state and the micro pairwise transmission, which has many roots: With more adopters in the system, the remaining individuals are more likely to follow the social norm as a result of psychology effect [10, 19, 20, 21] The utility of the product might increase because of network externalities (typical examples are telecommunication products like fax, social networks, and smartphone) [22, 23, 24]; At the same time, the product price might decrease with the decline of marginal cost due to economies of scale [6, 25, 26].

We operationalize the diffusion process through a Susceptible-Infectious-Recovered (SIR)-like model [16] where the transmissibility of the new product consists of two components. The first part is a constant representing the inherent attractiveness of the product, while the second part is proportional to the number of adaptors in the population, representing the macro-level social influence. By simulating this model on various empirical networks, we observe that the product can only occupy a viable market share when its transmissibility is larger than a critical value, analogous to the outbreak threshold of SIR model [16]. If the macro-level influence becomes strong enough, a shift of transition from continuous to discontinuous occurs. We use the tricritical point to refer to this threshold of macro-level influence. We further find that products tend to achieve higher market penetration and diffuse faster on networks with smaller tricritical values and vice versa.

Due to their implications, we focus on the critical and tricritical points and find that the former can be approximated with the outbreak threshold of SIR model. The latter, on the other hand, is closely related to the network localization strength [27, 28]. We propose a novel metric to measure such strength and demonstrate that our metric can accurately predict the tricritical point on a large corpus of empirical networks. The analytical expression of this metric automatically reveals its connection with the critical point and indicates a fundamental trade-off. While holding the network density (i.e., number of edges) constant, a larger critical value of the transmissibility would yield a smaller tricritical point value of the macro-level influence and vice versa. In other words, networks with stronger localization strength can facilitate the dissemination of less attractive products, yet lead to limited final market penetration. However, for networks with weaker localization strength, higher attractiveness is required for the product to spread out in an avalanche-like fashion, but the final market share tends to be larger. Guided by these findings, marketers can rewire the networks to fulfill their specific needs.

Model definition and behavior

Consider the scenario where a new product is released to a networked population with N individuals (nodes) and L connections (edges). Initially, most nodes are in the susceptible state (denoted by S) and may become adopted (denoted by A) after purchasing the product. The adopters may introduce the product to their susceptible neighbors and successfully convert them with a probability β' through social influence. Furthermore, with a probability μ , the adopters lose their interest in advertising the new product and become recovered (denoted by R). The dynamical process can be formulated as:

$$S_i(t-1) + A_j(t-1) \xrightarrow{\beta'} A_i(t) + A_j(t), \quad (1)$$

$$A_i(t-1) \xrightarrow{\mu} R_i(t), \quad (2)$$

where $Y_i(t)$ stands for node i in $Y \in \{S, A, R\}$ state at time t . The transmission occurs only if there exists a connection between node i and j . The diffusion process stops when all adopters vanish.

To incorporate both micro- and macro-level social influence documented in the literature [9, 10, 14], we assume that the transmissibility β' follows the expression below:

$$\beta'(t) = \min \left(1, \beta + \alpha \frac{R(t-1)}{N} \right), \alpha \geq 0, \beta' \in [0, 1]. \quad (3)$$

β represents the intrinsic attractiveness of the new product [1]; $\alpha \frac{R(t-1)}{N}$ quantifies the macro-level influence, indicating that susceptible individuals are more likely to accept the product with more recovered ones in the population. $R(t-1)$ is the number of recovered individuals in the system at time $t-1$ and α controls the strength of the macro-level influence. $\beta'(t)$ is further capped at one since it represents a probability. The whole model is illustrated in Figure 1(a).

To characterize the model behavior, we simulate it with different values of β and α on various empirical networks. The results on three networks are shown in Figure 1(b). We further adopt the dynamic message passing (DMP) method to theoretically track the final market penetration (i.e., $\frac{R(\infty)}{N}$). A good agreement between the theoretical predictions and simulations is illustrated in the figure. More details of the simulation rules and the DMP method are provided in the Methods section. Besides, a description of our network collection and supplementary results can be found in Supplementary Information.

Through extensive analyses, we identify several interesting phenomena. In the absence of macro-level influence, i.e., $\alpha = 0$, our diffusion model equates to the classical SIR model. As β increases above a critical value β_c , the system undergoes a continuous transition from the “vanished” state, where the new product fails to spread out, to the “prevalent” state, where a viable proportion of individuals finally adopts the product. When the macro-level social influence is strong enough, discontinuous transitions start to emerge, i.e., the market penetration level experiences a sudden jump as β increases [29]. In the meantime, the value of β_c remains stable despite the changes in α (see Supplementary Information for further analyses). This is reasonable since the macro-level influence can only manifest when there are adopters in the system, which requires $\beta \geq \beta_c$.

As expected, there is a critical value α_c above which the phase transition becomes discontinuous (see the plots with gray backgrounds in Figure 1(b)) [30, 31]. We define α_c as the tricritical point, whose value for a specific network can be numerically estimated (see

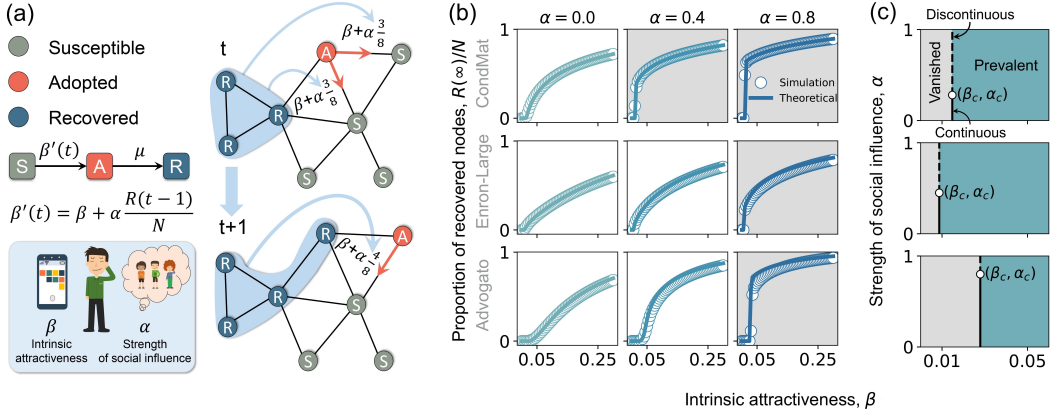


Figure 1: **Definition and behavior of the innovation diffusion model.** (a) Schematic diagram of the model and its spreading process on a toy network with eight nodes. The transmissibility $\beta'(t)$ of the SIR-like model is determined by the intrinsic attractiveness β of the new product and macro-level influence $\alpha \frac{R(t-1)}{N}$ together. At time t , the node in the adopted state is attempting to introduce the product to its two susceptible neighbors, and the contribution of macro-level influence to the transmissibility is $\alpha \frac{3}{8}$ since there are three recovered nodes in the system. At $t+1$, the intensity of macro-level influence becomes $\alpha \frac{4}{8}$ with one more recovered node added. (b) The market penetration, i.e., the final proportion of recovered nodes $R(\infty)/N$, for given α values as functions of β on three real-world networks (Advogato, Enron-Large, and CondMat networks). The dots and the solid lines represent the simulation and theoretical results obtained by the dynamic message passing (DMP) method. As the strength of macro-level influence increases, the diffusion processes start to exhibit discontinuous phase transitions (indicated by gray backgrounds). See the main text for details. (c) Phase diagrams for the same networks as (b). The diagrams are divided by the vertical line crossing the critical point β_c into the vanished and prevalent states. The product fails to secure a viable market share in the former state but becomes very popular in the latter state. The solid ($\alpha < \alpha_c$) and dashed lines ($\alpha > \alpha_c$) denote continuous (CT) and discontinuous transitions (DT), respectively, and intersect at the tricritical point indicated by the white dot.

the Methods section for details). The model behavior can thus be characterized by the tuple (β_c, α_c) that splits the phase space into different regions, as shown in Figure 1(c). Like β_c , which determines whether a product with a given intrinsic attractiveness β can successfully occupy the market, α_c also has real-world implications. Specifically, networks with smaller α_c values tend to facilitate higher market penetration and faster product diffusion (see analyses in Supplementary Information).

Quantifying the critical and tricritical points of phase transition

Due to the importance of β_c and α_c , estimating their values becomes crucial when studying innovation diffusion on networked population. Although it is possible to obtain their values

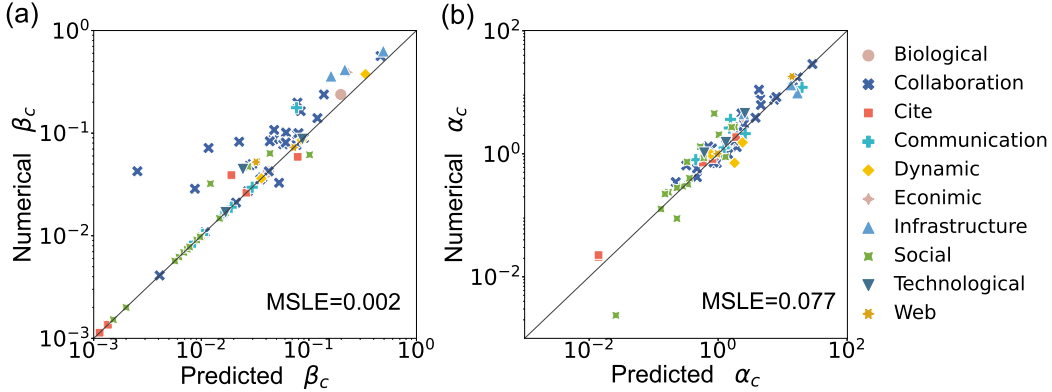


Figure 2: **Critical (β_c) and tricritical (α_c) points for real-world networks.** (a) Numerical values of β_c obtained through simulations versus the predicted values, i.e., equation (4). (b) Numerical values of α_c obtained through simulations versus the predicted values generated by equation (7). Each dot denotes a real-world network; solid diagonal lines of $y = x$ indicate an equality relationship between the predictions and the simulations. The mean squared logarithmic errors (MSLE) between the simulations and predictions are annotated in the plots.

numerically, running large amounts of repeated simulations can be computationally heavy (see the Methods section for details). Here, we show that the values of both β_c and α_c are determined by the network structure and have simple algebra expressions based on the so-called non-backtracking matrix \mathbf{B} [28].

In the previous section, we have established that the value of β_c is independent of the macro-level influence. Therefore, it can be approximated by the epidemic threshold of SIR model [32]:

$$\beta_c = \frac{\mu}{\rho(\mathbf{B}) + \mu - 1}, \quad (4)$$

where $\rho(\mathbf{B})$ denotes the largest eigenvalue of \mathbf{B} . For simplicity, we set μ to 1, so our predicted value for the threshold is $1/\rho(\mathbf{B})$. We compare the predicted and numerical values of the thresholds on 74 real-world networks in Figure 2(a). The results are mostly in agreement with each other, along with several exceptions reported before [33].

The case for α_c is more complicated. Compared to a continuous phase transition, much more susceptible individuals are converted to adopters simultaneously once β exceeds the threshold during a discontinuous phase transition, finally leading to an avalanche-like growth of recovered population. For this to happen, a positive feedback loop between more adopters (who will become recovered later) and larger transmissibility β' has to be established. The presence of macro-level influence alone is insufficient; considerable individuals in the system need to share similar probabilities of becoming adopters as well. While such probabilities typically vary from one individual to another since their connectivity patterns to others are different in most real-world networks [16, 34, 35]. For instance, a well-connected individual is more likely to be exposed to the new product and subsequently become an adopter than an individual with only a few neighbors in the network. Previous studies suggest that this probability can be quantified by the non-backtracking centrality [36, 37], which is defined

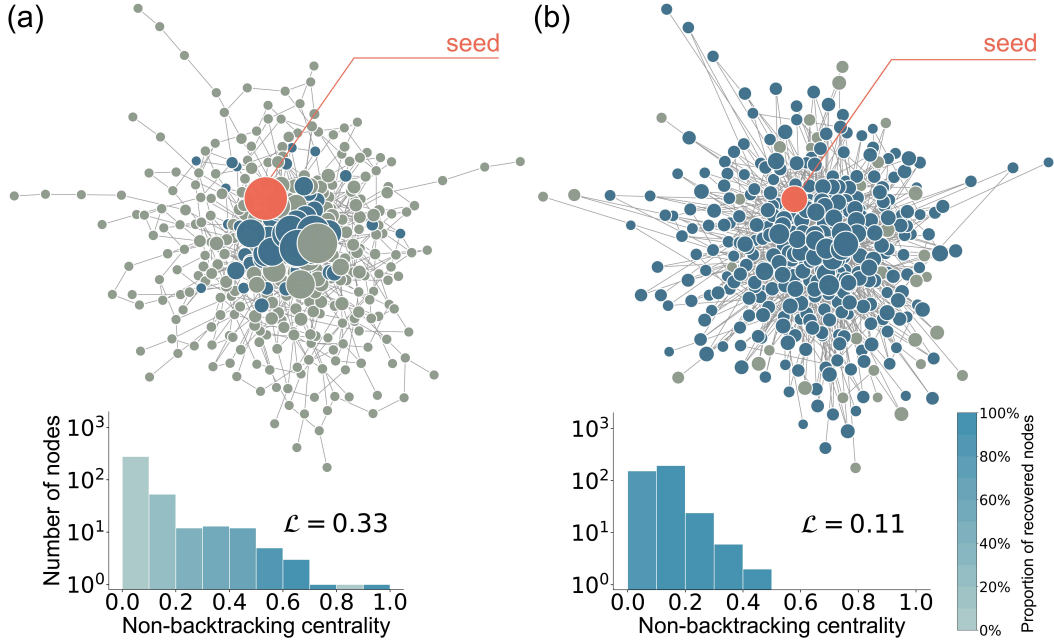


Figure 3: **Effect of network localization on innovation diffusion.** We simulate the product diffusion using the parameters $\alpha = 1$ and $\beta = \beta_c$ (the theoretical critical value) on two synthetic networks and visualize the outcomes in (a) and (b), respectively. The network in (b) is obtained by randomly rewiring the edges of the real-world network in (a) while preserving the degree sequence. The size of each node corresponds to its non-backtracking centrality. Gray (blue) colors represent the susceptible (recovered) final states; the initial seed is highlighted in red. The histograms show the distribution of node non-backtracking centrality, and the color of each bar indicates the proportion of recovered nodes in the corresponding bin. We annotate the values of \mathcal{L} for both networks in the figure. In terms of critical and tricritical values, we have $\beta_c = 0.104, \alpha_c = 1.17$ for (a) and $\beta_c = 0.183, \alpha_c = 0.58$ for (b).

as

$$x_i = \sum_j A_{ij} v_{j \rightarrow i}, \quad (5)$$

for node i . A_{ij} and $v_{j \rightarrow i}$ are the element of adjacency matrix \mathbf{A} and the component of principal eigenvector associated with the non-backtracking matrix \mathbf{B} , respectively.

Therefore, we hypothesize that it is easier for discontinuous phase transitions to take place on networks with smaller variance among their node centrality measures. To illustrate, we show the diffusion outcomes on two synthetic networks in Figure 3. Two networks have the same degree sequence, but the discrepancy in their connectivity patterns leads to different non-backtracking centrality distributions, tricritical points, and final states. Specifically, the network in Figure 3(a) has a small portion of nodes with much higher centrality indexes than other nodes, whereas the rewired network in Figure 3(b) has a more homogeneous centrality distribution. By definition, the network in (a) has a stronger

localization strength than that in (b). As a result, the recovered nodes in (a) tend to have larger centrality indexes, i.e., the diffusion is constrained to the central nodes, while the recovered nodes are scattered across the whole network in (b).

Based on this observation, we define the localization strength \mathcal{L} as:

$$\mathcal{L} = \frac{\sqrt{\frac{1}{N} \sum_{i=1}^N (x_i - \langle x_i \rangle)^2}}{\langle x_i \rangle \langle k \rangle}, \quad (6)$$

where the numerator is the standard deviation of node non-backtracking centrality measures. The denominator, i.e., the product of the average centrality value and the average degree, is added to ensure \mathcal{L} is comparable across different networks. We annotate the \mathcal{L} values for both networks in Figure 3 to illustrate that this metric can quantify the network localization strength.

By analyzing \mathcal{L} and α_c for different networks, we find a positive correlation between them. So we use the following formula to capture this relationship:

$$\alpha_c = \lambda \mathcal{L}^\eta, \quad (7)$$

where λ and η need to be determined empirically. To avoid overfitting on the real-world networks, we fit equation (7) on a collection of synthetic networks and obtain the results $\lambda = 2.63, \eta = 1.00$ (see the Methods section for details). We then compare the simulated values of α_c with their predicted values, i.e., $2.63\mathcal{L}$, for our collection of real-world networks in Figure 2(b) and find an excellent agreement. Using this relationship, one can easily predict the α_c value for any network as long as its topology is known, without the need to run extensive simulations. In practice, one can fit equation (7) directly on the real-world networks at hand for better estimates of λ and η ,

We note that there are other methods to quantify network localization strength. For instance, the inverse participation ratio (IPR) has been widely used in the literature for this purpose [28]. One can also replace x_i in equation (6) with eigenvector centrality [38], or use Gini coefficient to measure the variance [39]. However, the definition given by equation (6) provides the best predictions for α_c (see Supplementary Information for comparison).

Relationship between the critical and tricritical points

In addition to predicting the tricritical point, Equation (7) allows us to explore the relationship between β_c and α_c analytically. Specifically, on random uncorrelated networks, we have

$$\beta_c = \frac{1}{\langle k \rangle^3 (\alpha_c / \lambda)^{2/\eta} + \langle k \rangle - 1}, \quad (8)$$

where average degree $\langle k \rangle$ quantifies the edge density of the network. See the Methods section for the derivation of equation (8). Given all the networks considered have $\langle k \rangle > 2$, equation 8 suggests that β_c decreases monotonically with α_c and larger $\langle k \rangle$ can lead to smaller values for both β_c and α_c .

We mention earlier that a small β_c means that a less attractive product can still occupy the market while a small α_c indicates faster diffusion and higher market penetration. Therefore, the extent to which a real-world network can popularize the innovation i.e. its efficiency is negatively correlated with the values of β_c and α_c . To qualitatively give a

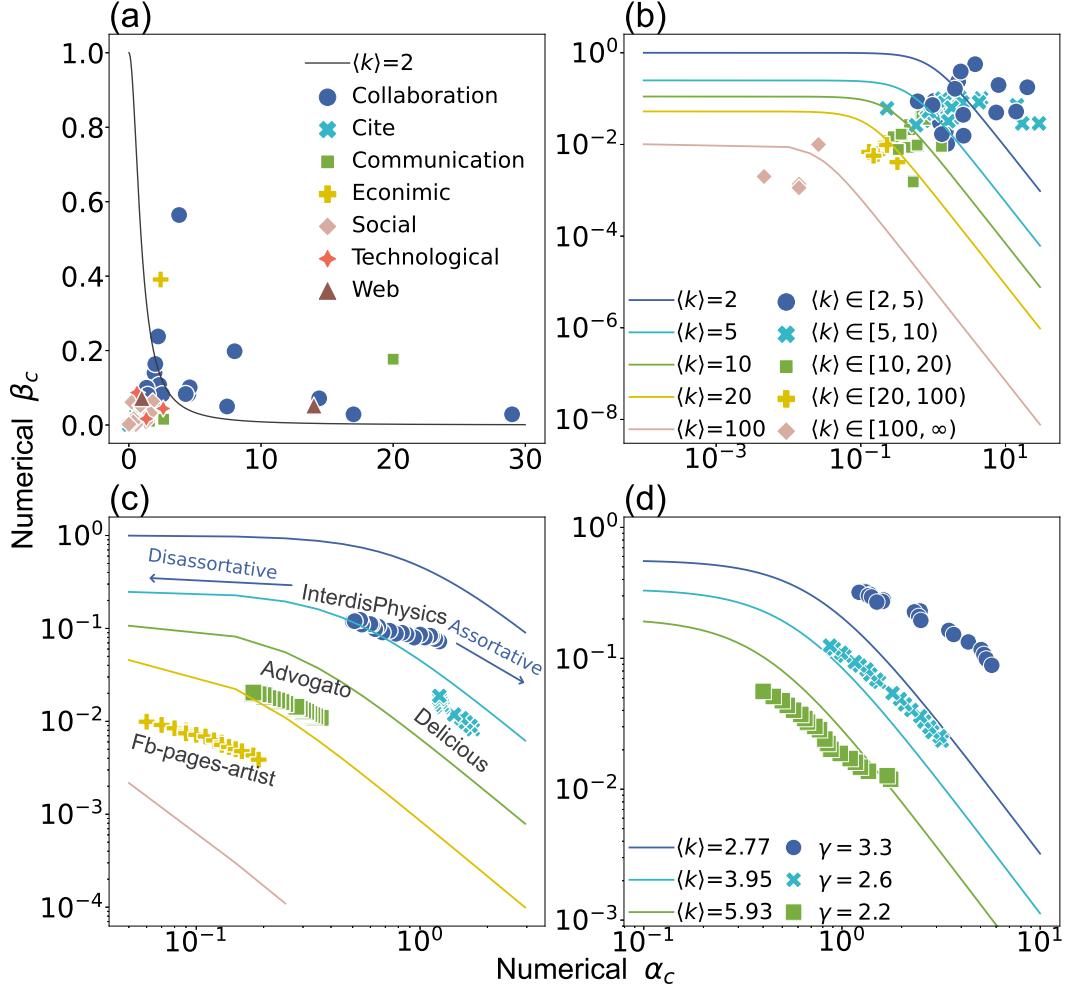


Figure 4: **Relationship between the critical and tricritical points.** β_c and α_c are obtained through numerical simulations. Each marker corresponds to a network, and its location indicates the corresponding critical and tricritical values. The solid lines represent the relationship between β_c and α_c described by equation 8 with given mean degree. (a) We plot equation 8 with $\langle k \rangle = 2$. (b) We mark the networks according to their average degree and show the lines corresponding to different $\langle k \rangle$ values. The plot is in log-scale to highlight the details. (c) By changing network assortativeness, we obtain configurations with different β_c and α_c values for four selected real-world networks (i.e., InterdisPhysics, Delicious, Advogato, Fb-pages-artist). The directions of the changes are annotated in the plot. (d) Same as (c) but with three instances of scale-free networks generated by the configuration model.

judgement of the efficiencies of real-world networks, in Figure 4(a), we plot a boundary through equation (8) with the limiting value $\langle k \rangle = 2$, together with markers of β_c and α_c for the collection of real-world networks. The boundary gives the performance of the sparsest tree-like network, to a great extent, and can thus be used to judge whether or not a network is effective. We observe that most networks reside below the boundary, which is also located close to the original point, and obviously effective. There are a handful of inefficient exceptions belonging to classes of collaboration, communication, economics, and Web. This is especially so for most collaboration networks, showing further distance to the origin of coordinates, given by relatively large α_c and small β_c . This pattern might be due to the negative effects of cultural or knowledge barriers in knowledge transfer [40]. It is evident that the efficiency of a real-world network can be roughly estimated by the inverse of its distance to the origin of the coordinate in plane of (β_c, α_c) .

We then reproduce Figure 4(a) in (b) using logarithmic scale to better observe the details. This time, we show the troughs for equation (8) with multiple $\langle k \rangle$ values, and color the networks based on the average degree brackets to which they belong. We find that most networks are located within the troughs predicted by equation (8), confirming our theory about the relationship between the critical and tricritical points.

Besides, this relationship has important implications. For the best diffusion outcome, one wishes β_c and α_c to be small simultaneously. According to equation (8), this can only happen on dense networks. It can also be concluded from the results reported in Figure 4 that the efficiency of a network, claimed to have negative correlation with the values of β_c and α_c , is positively associated with network density, but negatively associated with localization strength \mathcal{L} . Consequently, when the network density is fixed, equation (8) imposes a trade-off in popularizing the products. That is, strong localization (high \mathcal{L}) which causes smaller β_c can inevitably lead to larger α_c , and vice versa. Interestingly, the results in Figure 4 suggest that most empirical networks considered here strike a balance between β_c and α_c .

To reduce the value of β_c and α_c , one can consider adding edges to the network to increase its density. But when this is not feasible, we find that rewiring the network while preserving the edge density can also change the values of β_c and α_c . Here we demonstrate one effective approach, the Xalvi-Brunet & Sokolov algorithm [41], to achieve this goal. It was originally proposed to tune the assortativeness of the networks, but we find that it can also modify the localization strength (see the Supplementary Information for details). Specifically, increasing the assortativeness of the network can enhance its localization strength, further yielding larger α_c in exchange for smaller β_c . We show the results on four selected networks in Figure 4(c) and find that the constraint from equation (8) is still in effect during this process. The technique also works on synthetic networks, see examples in Figure. 4(d).

Discussion and outlook

In this paper, we study the innovation diffusion process on networked populations and reveal the fundamental topological structure that regulates this process. We focus on a model that encapsulates the micro-level pairwise transmission and macro-level influence observed in empirical studies. In the absence of the macro-level influence, the model exhibits a continuous phase transition from the vanished state to the prevalent state as we increase product attractiveness. The transition becomes discontinuous when the influence is strong enough. One main contribution is the finding that network localization strength regulates the innovation diffusion process by determining the critical and tricritical values. We provide

a novel analytical expression for localization strength, making it possible to estimate the tricritical point purely based on network topology. It advances a long line of modeling efforts to understand the impact of network structure on innovation diffusion from multiple research fields, including marketing, economics, and physics.

The critical and tricritical points have real-world implications: the former determines whether the product can occupy the market, and the latter determines the speed of diffusion and the final adoption rate. Ideally, one wishes to have small critical and tricritical values simultaneously. Our findings suggest that this can be achieved by adding more edges to the network. But when the edge density of the network is held constant, the relationship between the critical and tricritical points indicates that reducing one would increase the other.

Marketers can use our framework to create tailored marketing strategies. For products with high intrinsic attractiveness, they can choose a target population with relatively larger β_c . This could lead to a rapid occupation of the market with higher penetration. On the other hand, if the intrinsic attractiveness of the product is limited, then the ideal target population should have a smaller β_c . Even though the diffusion process is not as rapid and the final adoption rate is not as high, the product can at least secure a viable market share. Alternatively, one can also consider modifying the network structure for a fixed target population. For instance, adding new connections, i.e., channels of diffusion, to the network can effectively facilitate product diffusion. One can also adjust the connectivity patterns and trade one metric for the other to optimize the network for a specific product.

Our work leads to many exciting new research questions and lays the foundation for further exploration. For instance, we apply many assumptions and approximations while deriving the relationship between the critical and tricritical values, including treating all networks as random ones without degree correlation. This obviously fails to capture the features of real-world networks and leads to the discrepancy between the predicted and numerical results. How to accurately characterize such a relationship remains an open question. Another important direction is to develop cost-efficient network modification approaches to adjust the localization strength as needed. For instance, identifying a minimum set of edges that need to be added or rewired to achieve the goal is of great practical value.

Our findings also have potential applications beyond the innovation diffusion context. The localization phenomena play an essential role in many dynamical processes occurring on complex systems, especially epidemic spreading [27, 33]. Here we show that the newly proposed metric for quantifying localization strength works better than previous ones in predicting the position of the tricritical point. Moreover, its relatively simple algebra expression makes analytical treatment possible. It would be of particular interest to see what new insights it can bring when applied to different contexts.

Methods

Numerical simulations

In each realization, a node is randomly assigned the A state to initiate the diffusion, while the remaining nodes are in the S state. The diffusion process proceeds following the model rules until the absorbing state is reached, where no transmission can occur anymore. Throughout this paper, the recovery probability μ is set to 1.

In our model, the position of critical point β_c is numerically identified by searching for

the maximum value of the susceptibility

$$\chi = \frac{\sqrt{\langle r(\infty)^2 \rangle - \langle r(\infty) \rangle^2}}{\langle r(\infty) \rangle}. \quad (9)$$

For reliability, we perform 10^4 independent realizations to calculate the first-order and second-order moments of $r(\infty)$ on a given network with the same parameters.

To identify the value of α_c , we categorize the phase transitions into different classes by plotting the mass distribution of $r(\infty)$ near the predicted β_c values, with varying α for a large number of independent realizations. Discontinuous phase transitions occur if and only if the isolated peak of giant recovered clusters emerges [34]. Details and examples can be found in Supplementary Information.

Non-backtracking matrix and non-backtracking centrality

Since most of our theoretical analyses depend on non-backtracking matrix, here we provide a brief introduction to it. Considering an undirected network with L edges, its non-backtracking matrix \mathbf{B} is a $2L \times 2L$ non-symmetric matrix whose rows and columns denote directed edges $j \rightarrow i$ pointing from node j to i . And we have:

$$B_{z \rightarrow i, j \rightarrow z'} = \begin{cases} 1 & \text{if } z' = z, j \neq i, \\ 0 & \text{otherwise.} \end{cases} \quad (10)$$

When all nodes in the network belong to a strongly connected giant component, the non-backtracking matrix is non-negative and irreducible. According to the Perron-Frobenius theorem [42], there exists a positive leading eigenvector $v_{j \rightarrow i}$ associated to the largest eigenvalue λ_B :

$$\lambda_B v_{j \rightarrow i} = \sum_{k \rightarrow m} B_{j \rightarrow i, k \rightarrow m} v_{k \rightarrow m}. \quad (11)$$

The element $v_{j \rightarrow i}$ of the leading vector represents the centrality of node j while ignoring any contribution from the node i . The non-backtracking centrality of node i is defined as

$$x_i = \sum_j A_{ij} v_{j \rightarrow i}. \quad (12)$$

Unlike eigenvector centrality, non-backtracking centrality can reduce the effect of the ‘‘self-inflating’’ phenomenon associated with the hub nodes [28, 33].

Dynamic Message-Passing method

We use the dynamic message-passing method (DMP) to analytically treat the outbreak size and threshold. DMP has been used extensively in the context of contagion processes. It can prevent the contagion from backtracking to the source node, avoiding the mutual transmission effect [43, 44, 32]. Regardless of the initial conditions, DMP can accurately predict the probability of each node being in a specific state at time t , especially for tree-like networks.

First, let us derive the exact equations of DMP. The probabilities of node i being in S , A , or R states at time t are represented by $P_S^i(t)$, $P_A^i(t)$ or, $P_R^i(t)$, respectively. The three terms follow the constraint:

$$P_A^i(t) + P_S^i(t) + P_R^i(t) = 1. \quad (13)$$

The recovery process for an adopted node i is independent of its neighbors' state, and $P_R^i(t)$ can thus be represented as

$$P_R^i(t) = P_R^i(t-1) + \mu P_A^i(t-1). \quad (14)$$

Subsequently, the global quantity $R(t)$ can be obtained using

$$R(t) = \sum_i^N P_R^i(t). \quad (15)$$

Substituting equation (15) into equation (3), we have

$$\beta'(t) = \min \left(1, \beta + \alpha \frac{\sum_{i=1}^N P_R^i(t-1)}{N} \right), \quad (16)$$

which increases with $R(t-1)$ until it reaches the upper bound $\beta'(t) = 1$.

Next, $P_S^i(t)$ can be expressed as

$$P_S^i(t) = P_S^i(0) \Phi_i(t), \quad (17)$$

where $\Phi_i(t)$ denotes the probability that the product has not been successfully transmitted to node i from its adopted neighbors until time t . DMP assumes that the underlying network is tree-like and the state evolution of node i 's neighbors is independent. However, once node i is successfully persuaded by its neighbor z and switches to A state, it would attempt to convince another neighbor z' ($z' \neq z$). It gives rise to a dilemma because the state transitions of node z' and z are clearly correlated. To alleviate this issue, we assume that the focal node i is a cavity and define $\theta^{z \rightarrow i}(t)$ as the probability that node i has not been successfully persuaded by node z until time t . $\Phi_i(t)$ can then be factorized as $\prod_{z \in \partial i} \theta^{z \rightarrow i}(t)$ where ∂i is the neighbor set of node i . Substituting it into equation (17), we have

$$P_S^i(t) = P_S^i(0) \prod_{z \in \partial i} \theta^{z \rightarrow i}(t). \quad (18)$$

Message-passing is directional, meaning that $\theta^{i \rightarrow z}(t) \neq \theta^{z \rightarrow i}(t)$ for undirected networks. In our analysis, we treat each undirected edge as two directed edges pointing to opposite directions. Initially, we have $\theta^{z \rightarrow i}(0) = 1$ for all edges in the network. Later, $\theta^{z \rightarrow i}(t-1)$ decreases as the product transmits from node z to i , which occurs with the probability $\beta'(t) \phi^{z \rightarrow i}(t-1)$ where $\phi^{z \rightarrow i}(t-1)$ is the probability that the adjacent adopted node z has not passed the product to node i until time $t-1$. Hence, $\theta^{z \rightarrow i}(t)$ follows the updating rule:

$$\theta^{z \rightarrow i}(t) = \theta^{z \rightarrow i}(t-1) - \beta'(t) \phi^{z \rightarrow i}(t-1). \quad (19)$$

Now we need to find the expression for $\phi^{z \rightarrow i}(t)$. On the one hand, $\phi^{z \rightarrow i}(t)$ decreases when node z in A state recovers, or when the product is successfully transmitted from z to i , or when the two processes occur simultaneously. The corresponding probabilities for these events are μ , $\beta'(t)$, and $\mu\beta'(t)$, respectively. On the other hand, $\phi^{z \rightarrow i}(t)$ increases when node z in S state becomes A . The changing rate $\Delta P_S^{z \rightarrow i}(t)$ can be calculated as $P_S^{z \rightarrow i}(t-1) - P_S^{z \rightarrow i}(t)$ where $P_S^{z \rightarrow i}(t)$ represents the probability of node z staying in S state after interacting with the cavity node i . By combining all terms we have

$$\begin{aligned} \phi^{z \rightarrow i}(t) &= \phi^{z \rightarrow i}(t-1) - \beta'(t) \phi^{z \rightarrow i}(t-1) - \mu \phi^{z \rightarrow i}(t-1) + \mu \beta'(t) \phi^{z \rightarrow i}(t-1) + P_S^{z \rightarrow i}(t-1) - P_S^{z \rightarrow i}(t) \\ &= (1 - \beta'(t))(1 - \mu) \phi^{z \rightarrow i}(t-1) + P_S^{z \rightarrow i}(t-1) - P_S^{z \rightarrow i}(t). \end{aligned} \quad (20)$$

The next step is to express $P_S^{z \rightarrow i}(t)$ explicitly. Since node i is a cavity, node z will stay susceptible as long as it is not transferred by another neighbor j . Using equation (18), we can obtain the probability that z remains susceptible when its neighbor i is a cavity:

$$P_S^{z \rightarrow i}(t) = P_S^z(0) \prod_{j \in \partial z \setminus i} \theta^{j \rightarrow z}(t), \quad (21)$$

where $\partial z \setminus i$ represents the neighbors of z except for i . At $t = 0$, we have $P_S^{z \rightarrow i}(0) = 0$ if z is the seed that initiates the diffusion process and $P_S^{z \rightarrow i}(0) = 1$ otherwise. This can be represented as $P_S^{z \rightarrow i}(0) = 1 - \delta_{q_z(0), A}$ where $\delta_{q_z(0), A}$ is the Kronecker function and $q_z(0)$ represents the state of z at time $t = 0$.

Finally, we can employ equations (16), (19)-(21) to track the exact trajectory of $\theta^{z \rightarrow i}(t)$, $\phi^{z \rightarrow i}(t)$, and $P_S^{z \rightarrow i}(t)$ with the following initial conditions:

$$\theta^{z \rightarrow i}(0) = 1, \quad (22)$$

$$\phi^{z \rightarrow i}(0) = P_A^z(0) = \delta_{q_z(0), A}, \quad (23)$$

$$P_S^{z \rightarrow i}(0) = P_S^z(0) = 1 - \delta_{q_z(0), A}. \quad (24)$$

By further combining $P_R^i(0) = 0$ and $\beta(0) = \beta$ with equations (13), (14), (16), and (18)-(21) we can calculate the trajectory of $P_S^i(t)$, $P_A^i(t)$, $P_R^i(t)$, and obtain the order parameter $R(\infty)$. The computation complexity of DMP is $O(L)$, where L is the number of edges in the network.

Estimating the fitting parameters of localization strength

To characterize the relationship between localization strength \mathcal{L} and α_c , we first calculate their values for various network models and real-world networks (see Supplementary Information for details) and plot them. We find that one grows linearly with the other in the log-scale plots so we assume they follow the relationship $\ln \alpha_c = \eta \ln \mathcal{L} + \delta$, or $\alpha_c = \lambda \mathcal{L}^\eta$, $\lambda = e^\delta$. The values of η and δ need to be estimated from data. To avoid overfitting the real-world networks, we use the least square method to fit the relationship on a group of network models and obtain $\eta = 1$ and $\lambda = 2.63$. Therefore, we have $\alpha_c = 2.63 \mathcal{L}$. This allows estimating the value of α_c purely based on the network topology.

Relationship between the critical and tricritical points

With the analytical expressions of α_c and β_c , we can examine their relationship. For uncorrelated random networks, the element on the primary eigenvector in the non-backtracking matrix depends on the degree of nodes, see the equation (25) [33],

$$v_{j \rightarrow i} \sim k_j - 1. \quad (25)$$

The non-backtracking centrality for node i can then be approximated as

$$x_i = \sum_j A_{ij} v_{j \rightarrow i} \sim \sum_j \frac{k_i k_j}{N \langle k \rangle} (k_j - 1) = \frac{\langle k^2 \rangle - \langle k \rangle}{\langle k \rangle} k_i, \quad (26)$$

where we replace the A_{ij} with its expression in annealed networks, namely $\hat{A}_{ij} = k_i k_j / N \langle k \rangle$. The first-order moment of x_i can be expressed as

$$\langle x_i \rangle = \frac{\sum_i x_i}{N} \sim \langle k^2 \rangle - \langle k \rangle. \quad (27)$$

By substituting equations (26) and (27) into equation (6), we have

$$\mathcal{L} = \frac{\sqrt{\langle k^2 \rangle - \langle k \rangle^2}}{\langle k \rangle^2}. \quad (28)$$

This suggests that \mathcal{L} only depends on the first- and second-order moments of $\langle k \rangle$. Similarly, β_c can be represented as

$$\beta_c = \frac{\langle k \rangle}{\langle k^2 \rangle - \langle k \rangle}, \quad (29)$$

on annealed networks [33].

Combining equations (28) and (29), we have

$$\beta_c = \frac{1}{\langle k \rangle^3 \mathcal{L}^2 + \langle k \rangle - 1}. \quad (30)$$

And according to the relationship $\alpha_c = \lambda \mathcal{L}^\eta$, we obtain

$$\beta_c = \frac{1}{\langle k \rangle^3 (\alpha_c / \lambda)^{2/\eta} + \langle k \rangle - 1}. \quad (31)$$

Data availability

All data supporting this study are available on Mendeley Data (<https://data.mendeley.com/datasets/d848h7rcdg>) and are described in the Supplementary Information.

Code availability

The code to run numerical simulations and to plot the figure is available on GitHub (<https://github.com/LeyangXue/InnovationDiffusion>).

References

- [1] Everett M Rogers. *Diffusion of innovations*. New York: The Free Press, 2003.
- [2] Rabik Ar Chatterjee and Jehoshua Eliashberg. The innovation diffusion process in a heterogeneous population: A micromodeling approach. *Manage Sci*, 36(9):1057–1079, 1990.
- [3] Frances Stokes Berry and William D Berry. Innovation and diffusion models in policy research. *Theories of the policy process*, pages 253–297, 2018.
- [4] Gabriel E. Kreindler and H. Peyton Young. Rapid innovation diffusion in social networks. *Proc. Natl. Acad. Sci.*, 111:10881–10888, 2014.
- [5] Frank M Bass. A new product growth for model consumer durables. *Manage Sci*, 15(5):215–227, 1969.

- [6] Elmar Kiesling, Markus Günther, Christian Stummer, and Lea M Wakolbinger. Agent-based simulation of innovation diffusion: a review. *Cent Eur J Oper Res*, 20(2):183–230, 2012.
- [7] Joep WC Arts, Ruud T Frambach, and Tammo HA Bijmolt. Generalizations on consumer innovation adoption: A meta-analysis on drivers of intention and behavior. *Int. J. Res. Mark.*, 28(2):134–144, 2011.
- [8] Matthew O Jackson. *Social and economic networks*. Princeton university press, 2010.
- [9] Catherine SE Bale, Nicholas J McCullen, Timothy J Foxon, Alastair M Rucklidge, and William F Gale. Harnessing social networks for promoting adoption of energy technologies in the domestic sector. *Energy Policy*, 63:833–844, 2013.
- [10] Daire McCoy and Seán Lyons. Consumer preferences and the influence of networks in electric vehicle diffusion: An agent-based microsimulation in ireland. *Energy Res. Soc. Sci.*, 3:89–101, 2014.
- [11] Hazhir Rahmandad and John Sterman. Heterogeneity and network structure in the dynamics of diffusion: Comparing agent-based and differential equation models. *Manage Sci*, 54(5):998–1014, 2008.
- [12] Renana Peres, Eitan Muller, and Vijay Mahajan. Innovation diffusion and new product growth models: A critical review and research directions. *Int. J. Res. Mark.*, 27(2):91–106, 2010.
- [13] Jacob Goldenberg, Sangman Han, Donald R Lehmann, and Jae Weon Hong. The role of hubs in the adoption process. *J Mark*, 73(2):1–13, 2009.
- [14] Sebastiano A Delre, Wander Jager, Tammo HA Bijmolt, and Marco A Janssen. Will it spread or not? the effects of social influences and network topology on innovation diffusion. *J Prod Innov Manage*, 27(2):267–282, 2010.
- [15] Claudio Castellano, Santo Fortunato, and Vittorio Loreto. Statistical physics of social dynamics. *Rev. Mod. Phys.*, 81:591–646, May 2009.
- [16] Romualdo Pastor-Satorras, Claudio Castellano, Piet Van Mieghem, and Alessandro Vespignani. Epidemic processes in complex networks. *Rev. Mod. Phys.*, 87:925–979, Aug 2015.
- [17] Martin Hohnisch, Sabine Pittnauer, and Dietrich Stauffer. A percolation-based model explaining delayed takeoff in new-product diffusion. *Ind. Corp. Chang.*, 17(5):1001–1017, 2008.
- [18] Francis A Buttle. Word of mouth: understanding and managing referral marketing. *J. Strateg. Mark.*, 6(3):241–254, 1998.
- [19] H Peyton Young. Innovation diffusion in heterogeneous populations: Contagion, social influence, and social learning. *Am Econ Rev*, 99(5):1899–1924, 2009.
- [20] Ching-Wen Chen, Hung-Yi Chang, Juin-Han Chen, and Richard Weng. Elucidating the role of conformity in innovative smartphones. *Int. J. Mob. Commun.*, 14(1):56–78, 2016.

- [21] Douglas Guilbeault, Joshu Becker, and Damon Centola. *Complex Contagions: A Decade in Review*, pages 3–25. Springer International Publishing, Cham, 2018.
- [22] Michael L. Katz and Carl Shapiro. Product introduction with network externalities. *J Ind Econ*, 40(1):55–83, 1992.
- [23] Detlef Schoder. Forecasting the success of telecommunication services in the presence of network effects. *Inf. Econ. Policy*, 12(2):181–200, 2000.
- [24] Jeffrey H Rohlfs. *Bandwagon effects in high-technology industries*. MIT press, 2003.
- [25] Frederic M Scherer and David Ross. Industrial market structure and economic performance. *University of Illinois at Urbana-Champaign’s Academy for entrepreneurial leadership historical research reference in entrepreneurship*, 1990.
- [26] Edgar K Browning and Mark A Zupan. *Microeconomics: Theory and applications*. John Wiley & Sons, 2020.
- [27] A. V. Goltsev, S. N. Dorogovtsev, J. G. Oliveira, and J. F. F. Mendes. Localization and spreading of diseases in complex networks. *Phys. Rev. Lett.*, 109:128702, Sep 2012.
- [28] Travis Martin, Xiao Zhang, and M. E. J. Newman. Localization and centrality in networks. *Phys. Rev. E*, 90:052808, Nov 2014.
- [29] Ewa Lechman. Networks externalities as social phenomenon in the process ict diffusion. *Econ. Sociol.*, 11:22–40, 2018.
- [30] S Boccaletti, JA Almendral, S Guan, I Leyva, Z Liu, I Sendiña-Nadal, Z Wang, and Y Zou. Explosive transitions in complex networks’ structure and dynamics: Percolation and synchronization. *Phys. Rep.*, 660:1–94, 2016.
- [31] Raissa M D’Souza, Jesus Gómez-Gardenes, Jan Nagler, and Alex Arenas. Explosive phenomena in complex networks. *Adv. Phys.*, 68(3):123–223, 2019.
- [32] Andreas Koher, Hartmut H. K. Lentz, James P. Gleeson, and Philipp Hövel. Contact-based model for epidemic spreading on temporal networks. *Phys. Rev. X*, 9:031017, Aug 2019.
- [33] Romualdo Pastor-Satorras and Claudio Castellano. The localization of non-backtracking centrality in networks and its physical consequences. *Sci. Rep.*, 10(1):1–12, 2020.
- [34] Weiran Cai, Li Chen, Fakhteh Ghanbarnejad, and Peter Grassberger. Avalanche outbreaks emerging in cooperative contagions. *Nat. Phys.*, 11(11):936–940, 2015.
- [35] Peng-Bi Cui, Wei Wang, Shi-Min Cai, Tao Zhou, Ying-Cheng Lai, et al. Close and ordinary social contacts: How important are they in promoting large-scale contagion? *Phys. Rev. E*, 98(5):052311, 2018.
- [36] Munik Shrestha, Samuel V Scarpino, and Cristopher Moore. Message-passing approach for recurrent-state epidemic models on networks. *Phys. Rev. E*, 92(2):022821, 2015.
- [37] G Timár, SN Dorogovtsev, and JFF Mendes. Localization of nonbacktracking centrality on dense subgraphs of sparse networks. *arXiv preprint arXiv:2209.02594*, 2022.

- [38] Phillip Bonacich. Factoring and weighting approaches to status scores and clique identification. *J Math Sociol*, 2(1):113–120, 1972.
- [39] RB Bendel, SS Higgins, JE Teberg, and DA Pyke. Comparison of skewness coefficient, coefficient of variation, and gini coefficient as inequality measures within populations. *Oecologia*, 78(3):394–400, 1989.
- [40] Margaret L Sheng, Shen-Yao Chang, Thompson Teo, and Yuh-Feng Lin. Knowledge barriers, knowledge transfer, and innovation competitive advantage in healthcare settings. *Manag. Decis.*, 51(3):461–478, 2013.
- [41] R. Xulvi-Brunet and I. M. Sokolov. Reshuffling scale-free networks: From random to assortative. *Phys. Rev. E*, 70:066102, Dec 2004.
- [42] Roger A Horn and Charles R Johnson. *Matrix analysis*. Cambridge university press, 2012.
- [43] Brian Karrer and M. E. J. Newman. Message passing approach for general epidemic models. *Phys. Rev. E*, 82:016101, Jul 2010.
- [44] Andrey Y. Lokhov, Marc Mézard, Hiroki Ohta, and Lenka Zdeborová. Inferring the origin of an epidemic with a dynamic message-passing algorithm. *Phys. Rev. E*, 90:012801, Jul 2014.
- [45] Ryan A. Rossi and Nesreen K. Ahmed. The network data repository with interactive graph analytics and visualization. In *AAAI*, 2015.
- [46] Krzysztof J Cios and Lukasz A Kurgan. Trends in data mining and knowledge discovery. In *Advanced techniques in knowledge discovery and data mining*, pages 1–26. Springer, 2005.
- [47] Vladimir Batagelj and Andrej Mrvar. Analysis of large networks. In *Proceedings of Pajek Workshop at XXVI Sunbelt Conference*, 2006.
- [48] Jure Leskovec and Andrej Krevl. SNAP Datasets: Stanford large network dataset collection. <http://snap.stanford.edu/data>, June 2014.
- [49] Albert-László Barabási. *Network Science*. Cambridge University Press, 2016.
- [50] K.-I. Goh, B. Kahng, and D. Kim. Universal behavior of load distribution in scale-free networks. *Phys. Rev. Lett.*, 87:278701, Dec 2001.

Acknowledgements

This work was supported by the Key Program of the National Natural Science Foundation of China (Grant No. 71731002), by the National Natural Science Foundation of China (Grant Nos.), and by the Guangdong Basic and Applied Basic Research Foundation (Grant No. 2021A1515011975). We thank Claudio Castellano for the helpful comments and suggestions.

Author contributions

All authors have contributed equally to this article.

Competing interests

The authors declare no competing interests.

Supplementary information: network localization strength regulates innovation diffusion with macro-level social influence

1 Networks

We use various networks in this paper. Below we describe their sources and characteristics.

1.1 Real-world networks

We compile a large collection of real-world networks that facilitate innovation diffusion. They are from the following channels: (1) Network Repository¹ - NetRes [45]; (2) AMiner² [46]; (3) Pajek³ [47]; (4) American physical society⁴ - APS; (5) Index of Complex Network⁵ - ICN; (6) Stanford Network Analysis Project⁶ - SNAP [48]; (7) Github⁷; (8) Kaggle⁸; (9) Network Science by Albert-Laszlo Barabasi⁹ - Barabasi [49]; These networks describe connectivity patterns of different systems, including collaboration networks, citation networks, communication networks, technological networks, and social networks. We only keep the largest connected component from each network. The details of these networks can be found in Supplementary Table 1).

Table 1: Properties of real-world networks. We report network name, network type, number of nodes N , number of edges L , average degree $\langle k \rangle$, degree exponent γ estimated by the maximum likelihood method, degree correlation coefficient r , predicted critical point β_c , numerical critical point β_c^{num} , localization strength \mathcal{L} , predicted tricritical point α_c , numerical tricritical point α_c^{num} , and the source of networks.

Network	Type	N	L	$\langle k \rangle$	γ	r	β_c	β_c^{num}	\mathcal{L}	α_c	α_c^{num}	Source
bio-dmela	Biolog.	7,393	25,569	6.92	-5.06	-0.05	0.0419	0.0419	0.2923	0.7395	0.5800	NetRes
bio-yeast-protein-inter	Biolog.	1,458	1,948	2.67	-2.98	-0.21	0.1980	0.2380	0.9141	2.3126	1.7700	NetRes
ca-aminer	Collab.	942,212	3,808,259	8.08	-4.39	0.10	0.0088	0.0288	10.9531	27.7113	29.0000	NetRes
ca-BayesianNet	Collab.	554	1,238	4.47	-2.34	0.32	0.0471	0.0871	0.7152	1.8094	2.3400	Aminer
ca-citeseer	Collab.	227,320	814,134	7.16	-3.13	0.07	0.0117	0.0717	5.8610	14.8284	14.4000	NetRes
ca-CSphd	Collab.	1,025	1,043	2.04	-2.28	-0.25	0.4642	0.5642	1.4680	3.7140	3.8000	NetRes
ca-Data-Mining	Collab.	679	1,687	4.97	-3.02	0.12	0.0767	0.0767	0.3837	0.9708	1.2600	Aminer
ca-Database-System	Collab.	1,127	6,690	11.87	-2.76	0.21	0.0271	0.0271	0.1587	0.4014	0.4700	Aminer

Continued on next page

¹<https://networkrepository.com/>

²<https://www.aminer.cn/data/>

³<http://vlado.fmf.uni-lj.si/pub/networks/data/default.htm>

⁴<https://journals.aps.org/datasets>

⁵<https://icon.colorado.edu/#!/networks>

⁶<http://snap.stanford.edu/data/>

⁷<https://github.com/benedekrozemberczki/datasets>

⁸<https://www.kaggle.com/datasets/andrewlucchi/huawei-social-network-data>

⁹<http://networksciencebook.com/translations/en/resources/data.html>

Network	Type	N	L	$\langle k \rangle$	γ	r	β_c	β_c^{num}	\mathcal{L}	α_c	α_c^{num}	Source
ca-dblp-2012	Collab.	317,080	1,049,866	6.62	-3.26	0.27	0.0087	0.0287	6.6393	16.7974	17.0000	NetRes
ca-Information-Fusion	Collab.	348	595	3.42	-2.77	0.17	0.1379	0.2379	0.8439	2.1351	2.2100	Aminer
ca-Information-Retrieval	Collab.	657	1,907	5.81	-2.50	0.36	0.0424	0.0424	0.4814	1.2179	1.4400	Aminer
ca-Machine-Learning	Collab.	920	2,285	4.97	-3.68	0.09	0.0899	0.0899	0.3584	0.9068	1.0400	Aminer
ca-Semantic-Web	Collab.	671	2,237	6.67	-4.30	0.21	0.0528	0.0328	0.2687	0.6798	0.9500	Aminer
ca-Web-Services	Collab.	400	777	3.89	-3.46	0.14	0.1200	0.1400	0.4896	1.2387	1.9400	Aminer
ca-Erdos02	Collab.	5,534	8,472	3.06	-1.93	-0.04	0.0579	0.0779	0.6303	1.5947	2.0200	NetRes
ca-Erdos992	Collab.	4,991	7,428	2.98	-8.90	-0.45	0.0777	0.0977	1.0423	2.6369	1.7400	NetRes
ca-Math-compgeom	Collab.	3,621	9,461	5.23	-2.44	0.17	0.0369	0.0369	0.6281	1.5891	1.8000	Pajek
ca-MathSciNet	Collab.	332,689	820,644	4.93	-5.03	0.10	0.0298	0.0498	2.8769	7.2784	7.4300	NetRes
ca-AstroPh	Collab.	17,903	196,972	22.00	-4.50	0.20	0.0108	0.0108	0.1319	0.3337	0.2200	NetRes
ca-AstroPhysTechObs	Collab.	3,237	10,569	6.53	-6.01	0.29	0.0476	0.1076	1.7281	4.3721	2.3000	APS
ca-CondMat	Collab.	21,363	91,286	8.55	-3.35	0.13	0.0279	0.0479	0.4659	1.1788	0.8000	NetRes
ca-FluidDynamics	Collab.	7,252	18,514	5.11	-3.12	0.01	0.0801	0.1001	0.5367	1.3580	1.3400	APS
ca-GenTheoFiledParti	Collab.	10,949	30,364	5.55	-5.55	0.18	0.0428	0.0828	2.9702	7.5145	4.5000	APS
ca-GrQc	Collab.	4,158	13,422	6.46	-2.04	0.64	0.0225	0.0825	1.1689	2.9573	2.5200	NetRes
ca-HepPh	Collab.	11,204	117,619	21.00	-2.08	0.63	0.0041	0.0041	0.2463	0.6231	0.3200	NetRes
ca-InterdisPhysics	Collab.	2,360	5,745	4.87	-3.97	-0.01	0.0840	0.1640	0.8638	2.1854	2.0000	APS
ca-MaterialsSci	Collab.	12,438	41,912	6.74	-3.98	0.08	0.0613	0.1013	2.3635	5.9797	4.6000	APS
ca-MatMetPhy	Collab.	6,043	13,280	4.40	-4.29	0.01	0.0782	0.1982	3.1866	8.0621	8.0000	APS
ca-NetSci2019	Collab.	32,904	296,876	18.05	-2.02	0.99	0.0025	0.0425	0.5019	1.2699	0.7000	ICN
ca-NuclearAstroPhys	Collab.	1,500	7,715	10.29	-3.67	0.18	0.0354	0.0354	0.2746	0.6946	0.8500	APS
ca-StaPhyNonDyn	Collab.	24,732	68,793	5.56	-4.33	0.02	0.0433	0.0833	4.2011	10.6287	4.3000	APS
ca-Superconductivity	Collab.	20,161	118,150	11.72	-3.67	0.07	0.0210	0.0210	0.2199	0.5564	0.4700	APS
ca-TherProCondMat	Collab.	2,328	8,613	7.40	-3.36	0.08	0.0609	0.0809	0.3786	0.9578	1.4300	APS
cit-citeeer-2014	Cite	365,154	1,721,981	9.43	-2.72	-0.06	0.0190	0.0390	0.7111	1.7992	1.9000	ICN
cit-Database-System	Cite	1,350	4,055	6.01	-3.96	0.21	0.0787	0.0587	0.3131	0.7921	0.8200	Aminer
cit-DBLP	Cite	12,495	49,563	7.93	-3.35	-0.05	0.0263	0.0263	0.2745	0.6946	0.5800	NetRes
cit-HepPh	Cite	28,045	3,148,414	224.53	-4.49	0.63	0.0014	0.0014	0.0080	0.0202	0.0140	NetRes
cit-HepTh	Cite	22,721	2,444,642	215.19	-3.66	-0.03	0.0011	0.0011	0.0086	0.0218	0.0140	NetRes
email-dnc	Commun.	1,833	4,366	4.76	-1.86	-0.31	0.0297	0.0297	0.4747	1.2010	1.2400	NetRes
email-enron-large	Commun.	33,696	180,811	10.73	-1.97	-0.12	0.0087	0.0087	0.3048	0.7712	0.4500	NetRes
email-EU	Commun.	32,430	54,397	3.35	-4.25	-0.38	0.0190	0.0190	0.9989	2.5273	1.4900	NetRes
email-EuAll	Commun.	224,832	339,925	3.02	-2.78	-0.19	0.0103	0.0103	1.3831	3.4992	1.5600	SNAP
emails	Commun.	56,576	92,013	3.25	-1.89	-0.08	0.0155	0.0155	0.8091	2.0471	2.6300	Barabasi
phonecalls	Commun.	30,420	52,841	3.47	-4.71	0.17	0.0768	0.1768	4.5878	11.6071	20.0000	Barabasi
cs4	Dynamic	22,499	43,858	3.90	-3.27	0.32	0.3358	0.3758	0.2706	0.6845	1.8000	NetRes
ia-digg-reply	Dynamic	29,652	84,781	5.72	-3.52	0.00	0.0362	0.0362	0.3756	0.9502	0.7700	NetRes
ia-reality	Dynamic	6,809	7,680	2.26	-3.24	-0.68	0.0858	0.0858	0.5818	1.4719	2.4000	NetRes
econ-poli	Economic	2,343	2,667	2.28	-2.17	-0.34	0.2310	0.3910	1.4633	3.7021	2.4000	NetRes
inf-power	Infras.	4,941	6,594	2.67	-3.22	0.00	0.1606	0.3606	3.7297	9.4361	17.0000	NetRes
power-bcspwr10	Infras.	5,300	8,271	3.12	-8.58	-0.05	0.2160	0.4160	5.0446	12.7629	13.4000	NetRes
road-minnesota	Infras.	2,640	3,302	2.50	-4.80	-0.19	0.4920	0.6320	1.7043	4.3118	2.5000	NetRes
deezer-europe-edges	Social	28,281	92,752	6.56	-4.86	0.10	0.0435	0.0635	1.0388	2.6282	1.8000	Github
facebook-combined	Social	4,039	88,234	43.69	-2.51	0.06	0.0062	0.0062	0.0904	0.2288	0.1700	SNAP
lastfm-asia-edges	Social	7,624	27,806	7.29	-3.24	0.02	0.0272	0.0472	0.7767	1.9650	1.0300	Github
musae-DE-edges	Social	9,498	153,138	32.25	-2.55	-0.12	0.0069	0.0069	0.0482	0.1220	0.1300	SNAP
musae-facebook	Social	22,470	170,823	15.20	-3.19	0.08	0.0097	0.0097	0.3259	0.8246	0.6000	SNAP
soc-fb-Huawei	Social	1,000	50,153	100.31	-7.69	-0.01	0.0100	0.0100	0.0009	0.0023	0.0260	Kaggle
soc-musae-git	Social	37,700	289,003	15.33	-2.54	-0.08	0.0074	0.0074	0.1218	0.3083	0.3400	SNAP
soc-instagram-Huawei	Social	1,000	4,933	9.87	-12.02	0.01	0.1015	0.0615	0.0337	0.0853	0.2300	Kaggle
soc-academia	Social	200,167	1,022,440	10.22	-3.11	-0.02	0.0091	0.0091	0.3387	0.8569	1.3000	NetRes
soc-advogato	Social	5,054	39,374	15.58	-3.35	-0.10	0.0148	0.0148	0.1132	0.2864	0.2800	NetRes
soc-delicious	Social	536,108	1,365,961	5.10	-2.80	-0.07	0.0122	0.0322	1.0308	2.6079	1.6200	NetRes
soc-digg	Social	770,799	5,907,132	15.33	-1.70	-0.09	0.0015	0.0015	0.4968	1.2568	0.5300	NetRes
soc-fb-pages-artist	Social	50,515	819,090	32.43	-3.06	-0.02	0.0057	0.0057	0.0844	0.2136	0.1500	NetRes
soc-fb-pages-company	Social	14,113	52,126	7.39	-3.41	0.01	0.0327	0.0527	1.7180	4.3466	0.8700	NetRes
soc-fb-pages-government	Social	7,057	89,429	25.34	-3.06	0.03	0.0097	0.0097	0.1065	0.2693	0.2300	NetRes
soc-fb-pages-media	Social	27,917	205,964	14.76	-3.38	0.02	0.0168	0.0168	0.1528	0.3867	0.3600	NetRes
soc-Slashdot081106	Social	77,360	469,180	12.13	-3.51	-0.07	0.0078	0.0078	0.2810	0.7110	0.3300	NetRes
soc-twitter-Huawei	Social	1,000	250,315	500.63	-9.45	0.00	0.0020	0.0020	0.0001	0.0002	0.0046	Kaggle
tech-as-caida2007	Techno.	26,475	53,381	4.03	-2.09	-0.19	0.0168	0.0168	0.5819	1.4721	1.3200	NetRes
tech-p2p-gnutella	Techno.	62,561	147,878	4.73	-4.80	-0.09	0.0871	0.0871	0.3918	0.9912	0.6100	NetRes
tech-pgp	Techno.	10,680	24,316	4.55	-4.26	0.24	0.0244	0.0444	1.7170	4.3440	2.6000	NetRes
web-EPA	Web	4,253	8,897	4.18	-2.49	-0.30	0.0725	0.0725	0.3807	0.9631	0.9800	NetRes
web-webbase-2001	Web	16,062	25,593	3.19	-2.09	-0.10	0.0323	0.0523	6.8700	17.3811	14.0000	NetRes

1.2 Network models

We also generate a series of scale-free networks using different models. First, we create degree sequences by setting the degree exponent (γ) and minimum degree (k_{min}). Then we feed the sequence to the configuration model to create the networks while forbidding self-loops and multi-links. Since the edge density of the networks generated this way is very sensitive to the choice of γ , we set it to 3.3 for all instances and tune the edge density using k_{min} . To generate scale-free networks with varying γ values, we use the Goh-Kahng-Kim (GKK) algorithm [50]. The edge density of the networks generated by it is less sensitive to γ . We also apply the Xalvi-Brunet & Sokolov algorithm [41] to an instance of the networks generated by the configuration model to produce a series of scale-free networks with different assortativeness. The model has a key parameter p that defines the edge rewiring probability.

The parameters and the statistics of all synthetic networks can be found in Supplementary Table. 2. Since these networks are mainly used to fit the relation between α_c and \mathcal{L} , we only report the predicted values of β_c and numeric values of α_c .

Table 2: Properties of the network models. We report the generating method of the network, key parameter, number of nodes N , number of edges L , average degree $\langle k \rangle$, degree exponent γ , degree correlation coefficient r , predicted critical point β_c , localization strength \mathcal{L} , numerical tricritical point α_c^{num} .

Network	N	L	$\langle k \rangle$	γ	r	β_c	\mathcal{L}	α_c^{num}
CM ($k_{min} = 1$)	100,000	137,836	2.76	3.3	0.0006	0.2677	0.6572	1.48
CM ($k_{min} = 2$)	100,000	225,218	4.50	3.3	-0.0013	0.1353	0.3335	0.92
CM ($k_{min} = 3$)	100,000	313,560	6.27	3.3	-0.0033	0.0876	0.2255	0.72
CM ($k_{min} = 4$)	100,000	399,294	7.99	3.3	-0.0017	0.0717	0.1468	0.45
CM ($k_{min} = 5$)	100,000	492,157	9.84	3.3	-0.0030	0.0504	0.1325	0.46
CM ($k_{min} = 6$)	100,000	577,430	11.55	3.3	-0.0025	0.0481	0.0953	0.31
CM ($k_{min} = 7$)	100,000	660,324	13.21	3.3	0.0032	0.0438	0.0781	0.25
CM ($k_{min} = 8$)	100,000	752,652	15.05	3.3	-0.0016	0.0357	0.0728	0.26
CM ($k_{min} = 9$)	100,000	837,560	16.75	3.3	-0.0020	0.0334	0.0615	0.20
CM (Disassort, $p = 1.0$)	100,000	138,849	2.78	3.3	-0.0540	0.3248	0.6789	1.30
CM (Disassort, $p = 0.9$)	100,000	138,849	2.78	3.3	-0.0484	0.3214	0.6997	1.32
CM (Disassort, $p = 0.8$)	100,000	138,849	2.78	3.3	-0.0436	0.3193	0.6682	1.22
CM (Disassort, $p = 0.7$)	100,000	138,849	2.78	3.3	-0.0400	0.3078	0.6870	1.39
CM (Disassort, $p = 0.6$)	100,000	138,849	2.78	3.3	-0.0345	0.3010	0.6804	1.36
CM (Disassort, $p = 0.5$)	100,000	138,849	2.78	3.3	-0.0316	0.2945	0.6890	1.41
CM (Disassort, $p = 0.4$)	100,000	138,849	2.78	3.3	-0.0213	0.2789	0.7194	1.62
CM (Disassort, $p = 0.3$)	100,000	138,849	2.78	3.3	-0.0190	0.2714	0.6962	1.60
CM (Disassort, $p = 0.2$)	100,000	138,849	2.78	3.3	-0.0158	0.2688	0.6436	1.50
CM (Disassort, $p = 0.1$)	100,000	138,849	2.78	3.3	-0.0043	0.2300	0.8707	2.48
CM (Assort, $p = 0.1$)	100,000	138,849	2.78	3.3	0.0088	0.2087	0.8262	2.44
CM (Assort, $p = 0.2$)	100,000	138,849	2.78	3.3	0.0160	0.1946	0.8376	2.50
CM (Assort, $p = 0.3$)	100,000	138,849	2.78	3.3	0.0351	0.1634	1.0429	3.46
CM (Assort, $p = 0.4$)	100,000	138,849	2.78	3.3	0.0435	0.1519	1.0179	3.66
CM (Assort, $p = 0.5$)	100,000	138,849	2.78	3.3	0.0596	0.1333	1.1410	4.34
CM (Assort, $p = 0.6$)	100,000	138,849	2.78	3.3	0.0769	0.1165	1.2780	5.04
CM (Assort, $p = 0.7$)	100,000	138,849	2.78	3.3	0.0860	0.1070	1.3438	5.20
CM (Assort, $p = 0.8$)	100,000	138,849	2.78	3.3	0.0966	0.0988	1.4131	5.35
CM (Assort, $p = 0.9$)	100,000	138,849	2.78	3.3	0.1170	0.0884	1.5549	5.70
CM (Assort, $p = 1.0$)	100,000	138,849	2.78	3.3	0.1410	0.0770	1.7690	6.50

Continued on next page

Network	N	L	$\langle k \rangle$	γ	r	β_c	\mathcal{L}	α_c^{num}
GKK ($\gamma = 2.1$)	51,490	100,000	3.88	2.1	-0.1108	0.0109	0.7665	1.50
GKK ($\gamma = 2.2$)	57,539	100,000	3.48	2.2	-0.0783	0.0147	0.8748	2.25
GKK ($\gamma = 2.3$)	62,597	100,000	3.20	2.3	-0.0542	0.0201	0.9692	3.25
GKK ($\gamma = 2.4$)	66,554	100,000	3.01	2.4	-0.0345	0.0282	1.0284	3.26
GKK ($\gamma = 2.5$)	69,853	100,000	2.86	2.5	-0.0208	0.0415	1.0476	3.56
GKK ($\gamma = 2.6$)	72,258	100,000	2.77	2.6	-0.0123	0.0572	1.0701	3.81
GKK ($\gamma = 2.7$)	74,223	100,000	2.69	2.7	-0.0111	0.0849	1.0025	3.41
GKK ($\gamma = 2.8$)	75,961	100,000	2.63	2.8	-0.0030	0.1068	1.0280	3.28
GKK ($\gamma = 2.9$)	77,173	100,000	2.59	2.9	-0.0051	0.1403	0.9539	2.8
GKK ($\gamma = 3.0$)	78,203	100,000	2.56	3.0	0.0022	0.1635	0.9798	2.68
GKK ($\gamma = 3.1$)	79,005	100,000	2.53	3.1	-0.0010	0.2005	0.8992	2.16
GKK ($\gamma = 3.2$)	79,656	100,000	2.51	3.2	0.0003	0.2299	0.8220	1.74
GKK ($\gamma = 3.3$)	80,304	100,000	2.49	3.3	-0.0074	0.2685	0.6786	1.32
GKK ($\gamma = 3.4$)	80,884	100,000	2.47	3.4	0.0026	0.2774	0.7720	1.34
GKK ($\gamma = 3.5$)	81,390	100,000	2.46	3.5	-0.0005	0.3082	0.6222	1.17
GKK ($\gamma = 3.6$)	81,789	100,000	2.45	3.6	0.0033	0.3223	0.6329	1.11
GKK ($\gamma = 3.7$)	82,045	100,000	2.44	3.7	-0.0002	0.3392	0.6133	1.05
GKK ($\gamma = 3.8$)	82,637	100,000	2.42	3.8	0.0007	0.3560	0.5437	1.00
GKK ($\gamma = 3.9$)	82,819	100,000	2.41	3.9	-0.0023	0.3718	0.5233	0.92
GKK ($\gamma = 4.0$)	83,041	100,000	2.41	4.0	-0.0017	0.3840	0.4924	0.89

2 Supplementary results

2.1 Implications of the tricritical point

By definition, α is the intensity of the macro-level influence and α_c determines the phase transition class of the diffusion process. Here we show that α_c has further implications. Through simulations on the real-world networks, we find that networks with larger α_c values tend to have lower market penetration levels (Spearman's $\rho = -0.69, p < 0.001$, see Supplementary Figure 5(a)). We also examine the time required for 10% of the individuals to adopt the product and find a positive association between it and α_c (Spearman's $\rho = 0.74, p < 0.001$, see Supplementary Figure 5(b)). Given these correlations, a smaller α_c value is desirable for marketers.

2.2 The effect of macro-level influence on β_c

In the main text, we state that the introduction of the macro-level influence does not affect the value of β_c . We perform numerous simulations with varying α values on 38 empirical networks randomly selected from our collection to confirm this. We show the discrepancy between the numerical and theoretical values of β_c in Supplementary Figure 6. It appears that macro-level influence leads to β_c values that are larger than expected in some cases, but the difference decreases as the size of the network increases. This suggests that the finite-size effect is at play.

2.3 Other approaches to quantify the localization strength

Our main contribution is to show that the tricritical point is associated with the localization effect. Network localization refers to the phenomenon that the components x_i of an

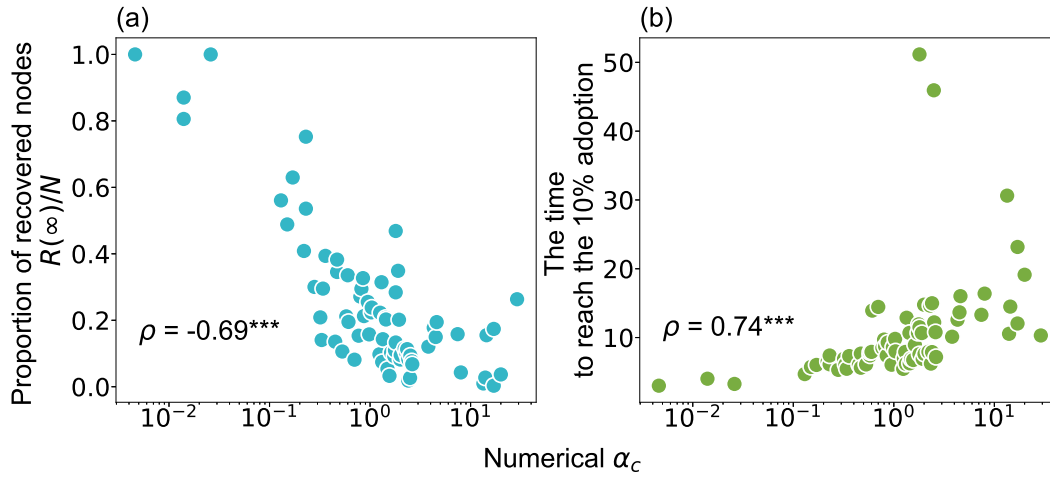


Figure 5: The implications of tricritical point α_c for real-world networks. (a) The final proportion of recovered nodes versus α_c . (b) The time needed for 10% individuals to adopt the product versus α_c . Each marker corresponds to an empirical network and the result is the average of 10,000 simulations with the parameter $(\beta_c+0.1, \alpha_c)$. The Spearman's correlation coefficients ρ are annotated in the figure. Both cases are statistically significant at the level 0.001.

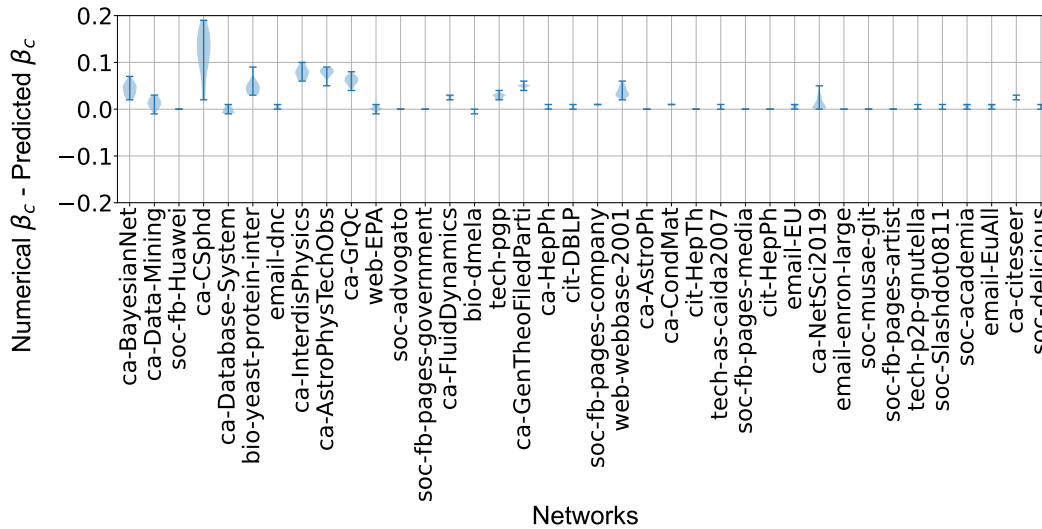


Figure 6: Discrepancy between the numerical and theoretical values of β_c . For each network, we run the simulations using different α values ranging from 0 to 1 and identify the β_c values. We then plot the distribution of the discrepancy between the numerical values and the theoretical value. The size of the network increases monotonically from left to right.

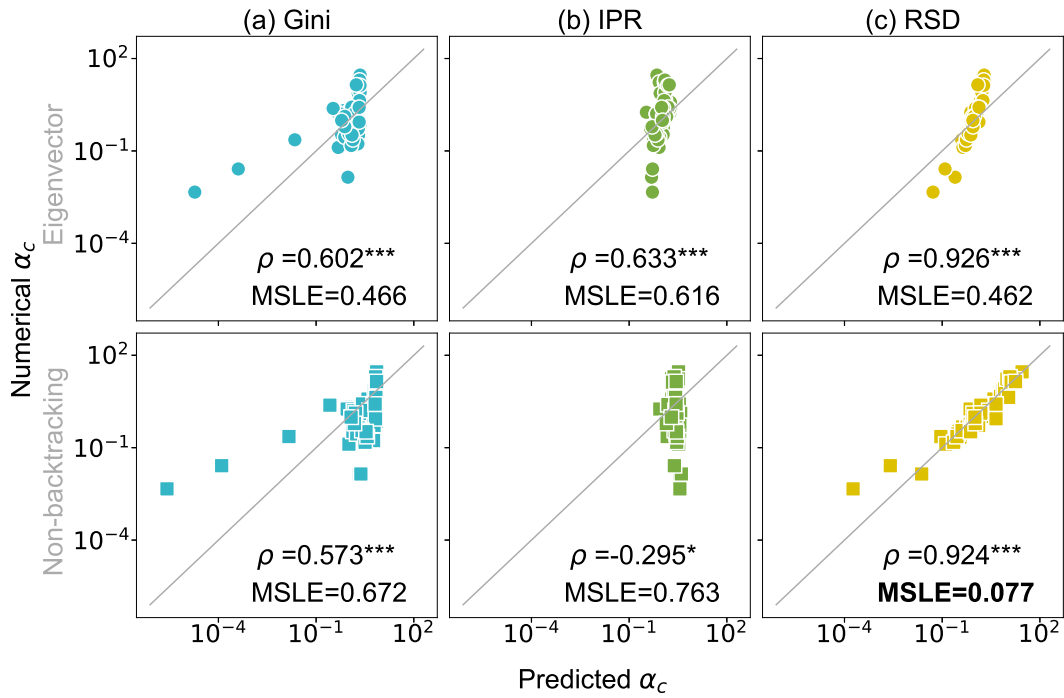


Figure 7: Comparison of different methods to predict the tricritical point. We combine the eigenvector and non-backtracking centrality measures with (a) Gini coefficient, (b) IPR, and (c) re-scaled standard deviation (RSD) to quantify the localization phenomenon of networks, respectively. Spearman's correlation coefficient ρ and the mean squared logarithmic errors (MSLE) between the numerical and predicted values of α_c are annotated in the plots (** $p < 0.001$, ** $p < 0.01$, * $p < 0.05$). The gray solid line $y = x$ is added to guide the eye.

eigenvector are concentrated on a subset of nodes. Considerable efforts have been devoted to studying the localization of the eigenvector and non-backtracking centrality due to their fundamental role in spreading dynamics. A common metric in the literature is inverse participation ratio (IPR), defined as $IPR = \sum_i x_i^4$. Instead of re-scaled standard deviation (RSD) proposed in the present work, one can also use the Gini coefficient to quantify the variance of x_i .

To show that our method works better in predicting the values of α_c , we compare the metric with other approaches. Here we consider two approaches to calculate node centrality: eigenvector and non-backtracking centrality and three approaches to measure the variance: IPR, RSD, and Gini coefficient, which lead to six different metrics. We fit their values against the numerical values of α_c on the network models to calculate the coefficients, then calculate the predicted values of α_c for the real-world networks. Two methods are adopted to evaluate the performance of different localization measures. First, we calculate Spearman's correlation coefficients between the numerical and predicted values. Second, since the α_c values for different networks have different magnitudes, we calculate the mean squared logarithmic error (MSLE). It is defined as

$$E = \frac{1}{m} \sum_{j=1}^m (\log(\alpha_{c,j}^{num} + 1) - \log(\alpha_{c,j} + 1))^2, \quad (2.1)$$

where $\alpha_{c,j}^{num}$ and $\alpha_{c,j}$ stand for the numerical and predicted tricritical points for network j .

We show the results in Supplementary Figure 7. We can see that all predicted values are positively correlated with the numerical values except for IPR of the non-backtracking centrality. The standard deviation approaches, both leveraging eigenvector and non-backtracking centrality, yield very high correlation coefficients. However, the one based on non-backtracking centrality has a much smaller MSLE. This comparison confirms that our proposed method is more accurate than other approaches.

2.4 Identifying the class of phase transition

To identify the numerical tricritical point, we plot the distribution of probabilities of observing adopter clusters of different sizes at β_c while varying the value of α . See Supplementary Figure 8 for the examples on the soc-fb-pages-artist network. The dots that follow a power-law distribution in the figure correspond to the premature clusters of adopters that die out in the early stage of diffusion. When α is close to 0.15, a spike of mass distribution on the right-hand side starts to emerge. These dots represent the giant clusters of adopted individuals, which occupy a finite fraction of the system. The phase transition is discontinuous when the giant clusters are well separated from the premature ones and this is how we determine the critical value α_c .

2.5 Relation between predicted critical and tricritical point

To examine the relation between β_c and α_c , we show the scatter plot of their numerical values obtained from different real-world networks in the main text. Here we show their predicted values in Supplementary figure 9(a), the patterns are qualitatively similar to those in the main text.

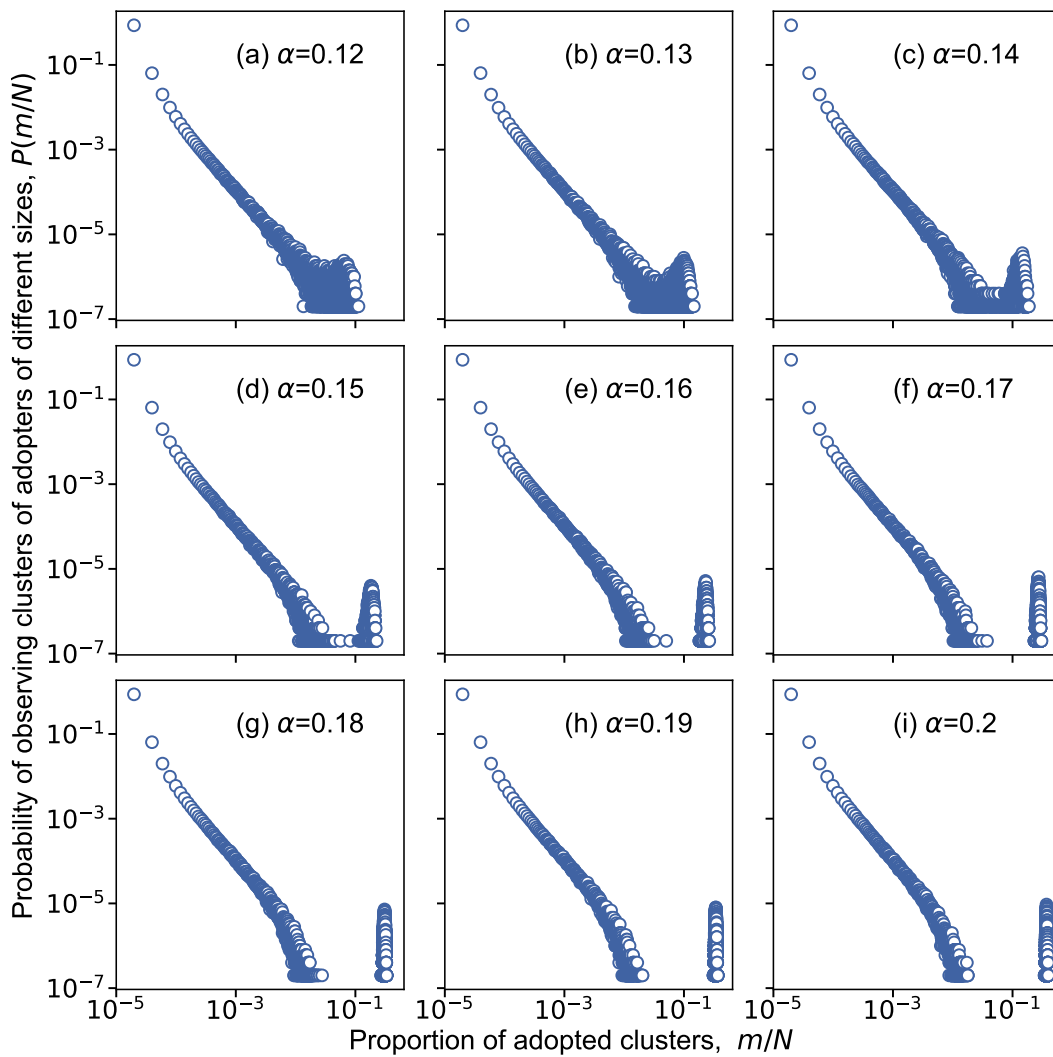


Figure 8: Probabilities of observing adopter clusters of different sizes with different α values on the soc-fb-pages-artist network. For a pair of parameters (β_c, α) , we perform 5×10^6 simulations to calculate the probability of forming the clusters with different sizes. m denotes the size of adopter clusters.

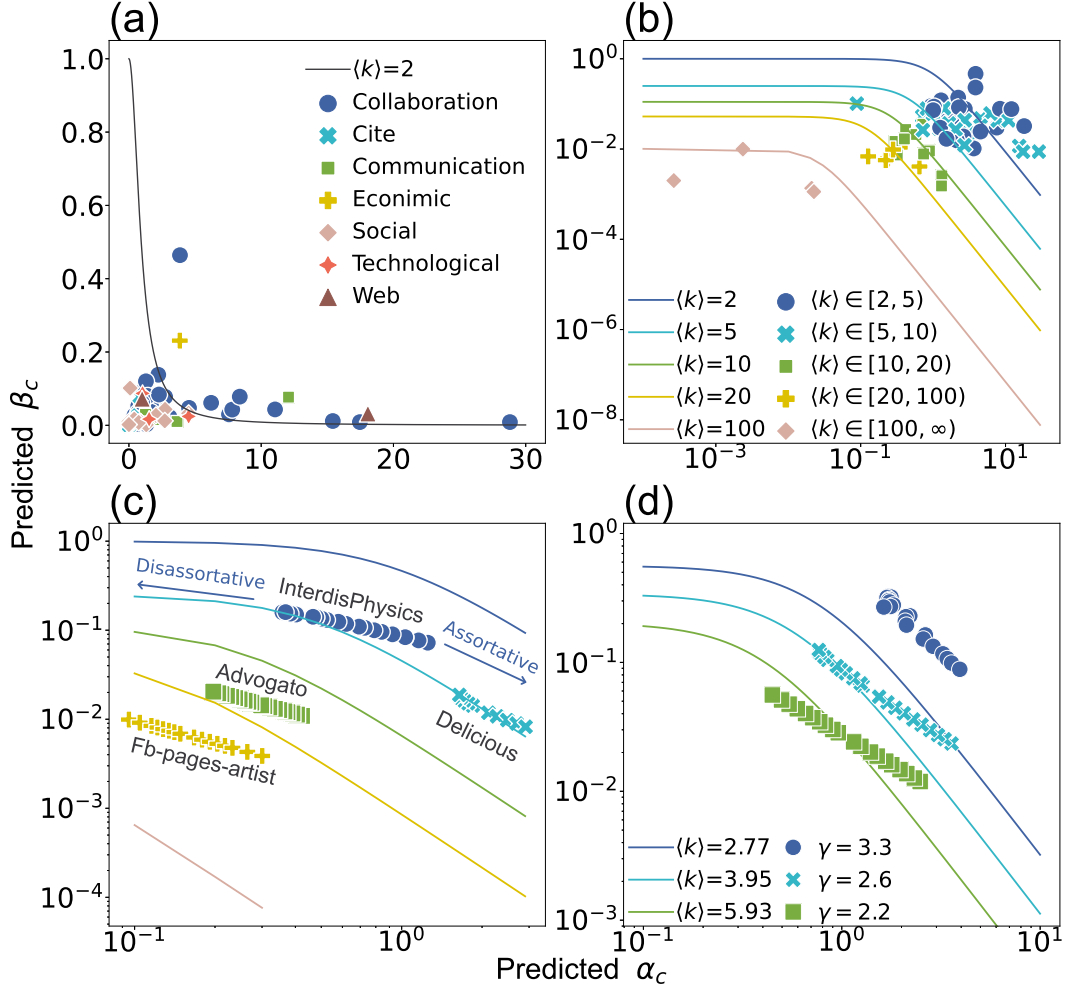


Figure 9: **Relationship between the critical and tricritical points.** β_c and α_c are obtained theoretically from Eq. (4) and Eq. 7, respectively. Each dot corresponds to a network and its location indicates the critical and tricritical values obtained from predicted results. The solid line represents the relation between β_c and α_c described by Eq. 8 with a given mean degree. (a) We mark the categories of the networks and show the line with $\langle k \rangle = 2$. (b) We mark the networks according to their average degree and show the lines corresponding to different $\langle k \rangle$ values. The plot is in log-scale to highlight the details. (c) By changing the network's assortativeness, we obtain configurations with different β_c and α_c values for four selected real-world networks (i.e., InterdisPhysics, Delicious, Advogato, Fb-pages-artist). The directions of the changes are annotated in the plot. (d) Same as (c) but with three instances of scale-free networks generated by the configuration model.

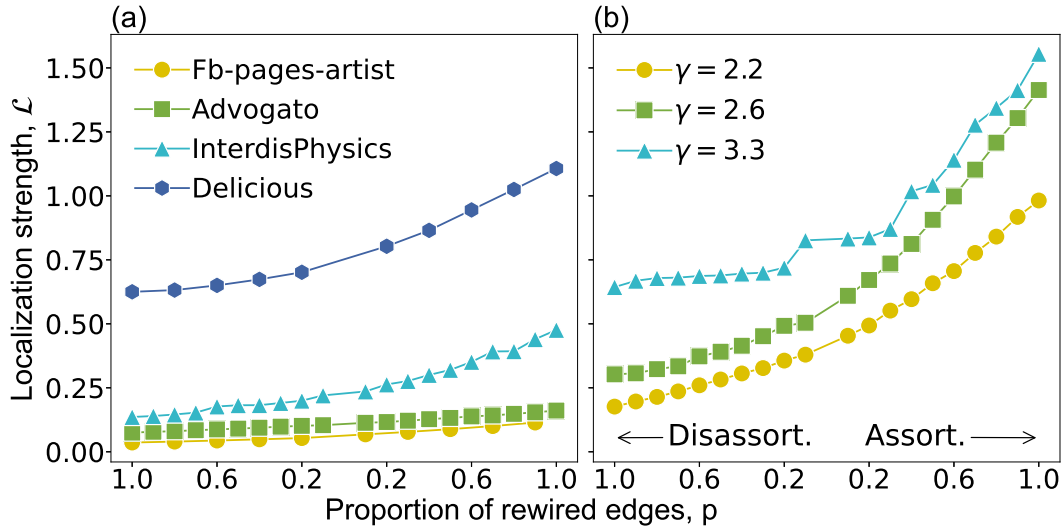


Figure 10: Varying the localization strength of networks by tuning the magnitude of degree correlation. We apply the Xalvi-Brunet & Sokolov algorithm with different portions of rewired edges on (a) four real-world networks (Fb-pages-artist, Advogato, InterdisPhysics, Delicious) and (b) three instances of scale-free networks generated by configuration model with minimum degree $k = 1$ and different γ values.

2.6 Tuning the localization strength of network

We present an approach to tune the localization strength of the network by changing the degree correlation through the Xalvi-Brunet & Sokolov algorithm. It works by selecting two edges at random and ordering the four nodes at the ends of the edges according to their degree for rewiring. If the goal is to increase the assortativity, the algorithm connects the two nodes with the highest degree and the two with the lowest degree. Conversely, the node with the highest degree is connected to the one with the lowest degree. To tune the magnitude of degree correlation, we execute the deterministic rewiring step with probability p , and randomly pair the four nodes with the probability $1 - p$. By fixing the total number of rewired steps, we can generate the network with different magnitudes of degree correlation by varying p . The results for four real-world networks and three synthetic networks are shown in Supplementary Figure 10. The localization strength increases with the network assortativity level.